ISSN 1068-1620, Russian Journal of Bioorganic Chemistry, 2020, Vol. 46, No. 3, pp. 448–457. © Pleiades Publishing, Ltd., 2020.

LETTER TO THE EDITOR

Essential Structural Profile of Novel Adenosine Derivatives as Antiplatelet Aggregation Inhibitors Based on 3D-QSAR Analysis Using CoMFA, CoMSIA, and SOMFA

Shunlai Li[a], XueFeng Bao[a], Chenghu Lu[a], Chaorui Ren[a], Guocheng Liu[a], and Hongguang Du[a, 1]

[a]*College of Science, Beijing University of Chemical Technology, Chaoyang District, Beijing, 100029 China*

Received June 11, 2019; revised August 23, 2019; accepted December 29, 2019

Abstact—In this study, comparative molecular field analysis (CoMFA), comparative molecular similarity indices analysis (CoMSIA), and the self-organizing molecular field analysis (SOMFA) were performed on a series of novel adenosine derivatives. Significant correlation coefficients (CoMFA, $q^2 = 0.560$, $r^2 = 0.940$, F value = 71.850, and SEE = 0.097; CoMSIA, $q^2 = 0.528$, $r^2 = 0.943$, F value = 29.29 and SEE = 0.108; SOMFA, $r^2 = 0.615$, $r^2_{cv} = 0.577$, F value = 60.797, and SEE = 0.226) were obtained, and the generated models were validated using test sets. By analyzing the corresponding contour maps in detail, new adenosine derivatives with potential efficacy were designed for synthesis in the future.

Keywords: adenosine derivatives, design, antiplatelet aggregation activity, 3D-QSAR, CoMFA

DOI: 10.1134/S1068162020030103

The leading cause of stroke [1], coronary heart disease (CHD) [2, 3], is a huge threat to public health worldwide, and antiplatelet drugs (antithrombotic drugs) produce remarkable treatment effects in this field [4]. Some antiplatelet drugs have been discovered and applied in clinical treatment, such as aspirin, clopidogrel, ticlopidine, platelet fibrinogen receptor antagonists, and ticagrelor [5]. However, some causes, such as the resistance of aspirin and clopidogrel, bigger side effect of bleeding, and high cost of fibrinogen receptor antagonists, hindered the curative effects of antiplatelet drugs [6, 7]. Under the previous guidance and experience, some novel drugs need to be further studied to make up the inadequacy of current drugs. As approved for patients with acute coronary syndrome (ACS) and myocardial infarction (MI) in 2012, ticagrelor (the structure shown in Fig. 1) [8] hinders ADP binding to $P2Y_{12}$ receptors in a direct and reversible manner, resulting in faster work, migration profiles and genetic polymorphisms induce low pharmacokinetic changes. Although it is effective in reducing the mortality of cardiovascular patients, a non-fatal higher bleeding rate marked a significant adverse side effect of ticagrelor [8]. It is noteworthy that cangrelor (as shown in Fig. 1) [9], which was developed in 1999, has a significant effect on antiplatelet aggregation and a higher antiplatelet activity than clopidogrel. Meanwhile, it can rapidly inhibit platelet aggregation and produce activity without the metabolism, better controlling the bleeding time [10]. However, for the moderately high bleeding, it is worth to further optimize its chemical structure and improve its activity. According to the pharmacodynamic action, it is necessary and urgent to further develop antiplatelet drugs with better curative effect and lower side-effects for the treatment of stroke, coronary heart disease, and thrombosis.

In order to dig out helpful information in designing more highly active and safe drugs, the analysis of quantitative structure activity relationship (QSAR) [11–15], which predicts biological activity based on chemical structures, could provide important basic information. Three-dimensional quantitative structure activity relationship (3D-QSAR)analysis methods, such as comparative molecular field analysis (CoMFA) [16], comparative molecular similarity indices analysis (CoMSIA) [17], and the self-organizing molecular field analysis (SOMFA) [18] are well-known methods in analysis of compounds.

A series of N^6-alkyl(aryl)-2-alkyl(aryl)thio-adenosines have been synthesized and their antiplatelet activity has been evaluated by our research group [19]. The structures and activities described by IC_{50} (μM) are shown in Table 1, and the synthetic route is shown in Scheme 1. In this paper, 3D-QSAR analysis on these adenosine compounds was carried out by CoMFA, CoMSIA, and SOMFA methods. According to the final 3D-QSAR analysis, some structural helpful information in enhancing the platelet inhibitory activity was obtained and twenty novel adenosine

[1] Corresponding author: phone/fax: +86-10-64439218; e-mail: dhg@mail.buct.edu.cn.

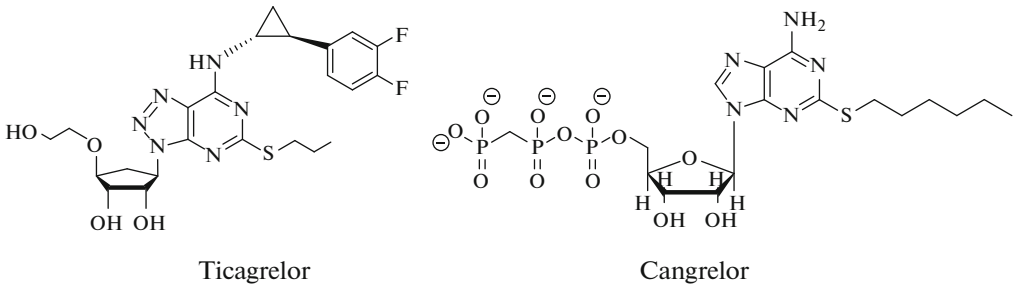

Fig. 1. Structures of ticagrelor and cangrelor.

derivatives with potential antiplatelet efficacy were designed for synthesis in future.

The data set consisted of 45 adenosine derivatives, which were taken from our research paper [19], was subjected to 3D-QSAR analysis using CoMFA, CoMSIA, and SOMFA. The forty five compounds with experimental data were divided randomly into training set and test set in a ratio of about 8 : 1, in which the training set contained 40 compounds (80%) and the test set contained 5 compounds (20%). The 50% inhibiting concentration IC_{50} values were translated into the PAC values using the equation $PAC = IC_{50} \times 50/300$. Lower PAC value indicated greater inhibitory activity. Then PAC values were translated into $\log(PAC) = \log((1/PAC)/(300 \times 10^{-6}))$.

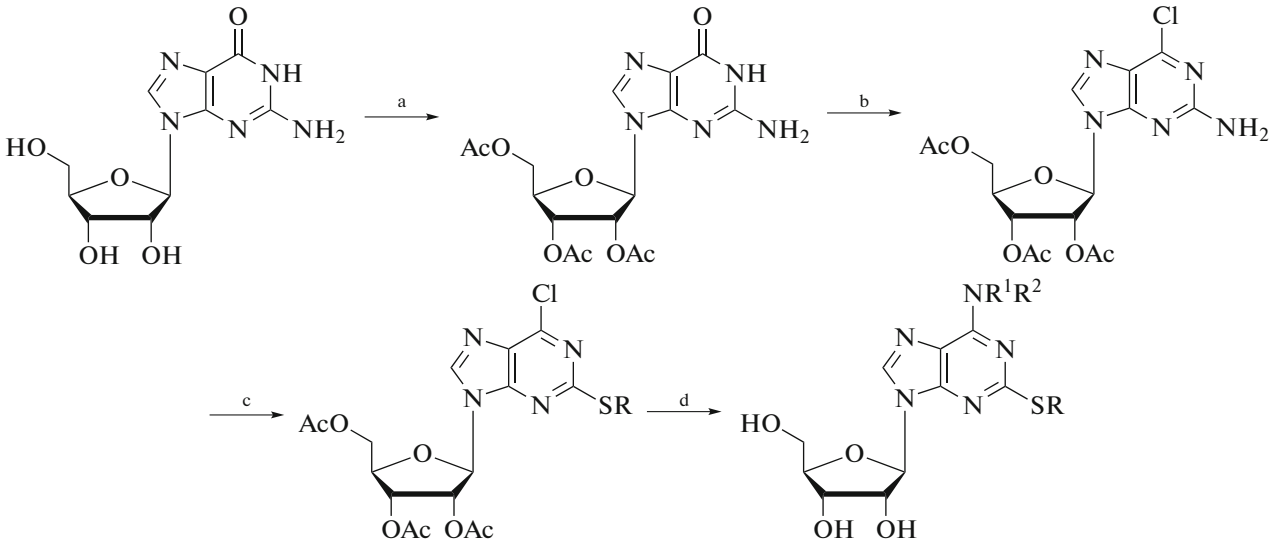

R = alkyl, aryl; R^1 = alkyl, aryl; R^2 = H or R^1

Scheme 1. Synthesis of N^6-alkyl(aryl)-2-alkyl(aryl)thioadenosines. Reagents and conditions: (a) Ac_2O, DMAP, Et_3N, CH_3CN, r.t.; (b) $POCl_3$, Et_4NCl, *N*,*N*-dimethylaniline, CH_3CN, reflux; (c) isoamyl nitrite, MeCN, RSSR, 60°C; (d) 1) HNR^1R^2, Et_3N, EtOH, reflux; 2) Na, reflux.

All 3D chemical structures of the 45 compounds were drawn and energy-minimized in SYBYLx1.3 [20] using the MMFF94s force field with Delre charges [21]. The alignment of molecules is a very considerable factor for 3D-QSAR studies. In our study, three different kinds of alignment were selected to define overlap. The first superposition of molecules, which was based on purine ring as common structure (alignment A), is displayed in Fig. 2. The second superposition, which was based on using adenosine ring as common structure (alignment B), is displayed in Fig. 3. The third superposition, which was based on the best conformation in the receptor (alignment C), is displayed in Fig. 4.

The CoMFA method was performed on molecular alignment to generate the 3D-QSAR model. Adjusting column filtering from 0.5 to 5 kcal/mol would improve efficiency and decrease the noise. Cutoff values of two CoMFA descriptors were changed at some point from 10 to 50 kcal/mol to cut the large steric domination and minimize electrostatic energies. The remaining parameters are the system defaults.

Table 1. The structures of adenosine derivatives and their experimental and predictive activities

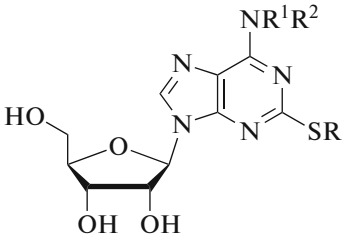

Entry	Compd.	R	R^1	R^2	IC_{50}, μM[a]	PAC (%, 300 μM) [c]	log(PAC)	Predicted log(PAC)		
								CoMFA	CoMSIA	SoMFA2
1	$5a_1$	Et	n-C_6H_{13}	H	Nc[b]	57.0	3.767	3.748	3.794	3.697
2	$5a_5$	Et	c-C_6H_{11}	H	104 ± 7	17.3	4.284	4.251	4.295	3.991
3	$5a_3$	i-Pr	n-C_6H_{13}	H	Nc	72.0	3.666	3.608	3.208	3.746
4	$5a_4$	n-Bu	n-C_6H_{13}	H	Nc	66.0	3.703	3.730	3.723	3.708
5*	$5a_2$	n-Pr	n-C_6H_{13}	H	102 ± 11	17.0	4.292	3.720	3.738	3.759
6	$5a_6$	n-Pr	c-C_6H_{11}	H	151 ± 9	25.2	4.122	4.182	4.146	4.071
7	$5a_7$	i-Pr	c-C_6H_{11}	H	187 ± 15	31.2	4.029	4.135	4.125	3.990
8	$5a_8$	n-Bu	c-C_6H_{11}	H	83 ± 4	14.8	4.382	4.189	4.23	3.996
9	$5a_9$	Et	n-Bu	n-Bu	Nc	77.0	3.636	3.642	3.635	3.698
10	$5a_{10}$	n-Pr	n-Bu	n-Bu	Nc	86.0	3.588	3.562	3.582	3.490
11	$5a_{11}$	n-Bu	$CH_3OCH_2CH_2$	H	63 ± 5	10.5	4.502	4.499	4.501	4.101
12	$5b_1$	Me	CH_2Ph	H	Nc	52.0	3.807	3.934	3.921	3.878
13	$5b_2$	Et	CH_2Ph	H	176 ± 16	29.3	4.056	4.011	4.027	3.939
14	$5b_3$	n-Pr	CH_2Ph	H	181 ± 14	30.2	4.043	4.984	3.997	3.914
15*	$5b_4$	n-Bu	CH_2Ph	H	202 ± 20	33.7	3.996	4.004	3.989	3.786
16	$5b_5$	Me	p-$MePhCH_2$	H	Nc	77.0	3.636	3.614	3.569	3.742
17	$5b_6$	Et	p-$MePhCH_2$	H	Nc	88.0	3.578	3.620	3.671	3.604
18	$5b_7$	n-Pr	p-$MePhCH_2$	H	Nc	70.0	3.678	3.614	3.615	3.608
19	$5b_8$	n-Bu	p-$MePhCH_2$	H	Nc	89.0	3.574	3.569	3.606	3.632
20	$5b_9$	Me	p-$MeOPhCH_2$	H	Nc	69.0	3.684	3.704	3.698	3.651
21	$5b_{10}$	Et	p-$MeOPhCH_2$	H	Nc	74.0	3.654	3.817	3.814	3.703
22	$5b_{11}$	n-Pr	p-$MeOPhCH_2$	H	216 ± 12	36.0	3.967	3.724	3.712	3.758
23	$5b_{12}$	n-Bu	p-$MeOPhCH_2$	H	Nc	82.0	3.609	3.673	3.681	3.582
24	$5b_{13}$	Me	$PhCH_2CH_2$	H	36 ± 5	6.0	4.745	4.681	4.736	4.289
25*	$5b_{14}$	Et	$PhCH_2CH_2$	H	29 ± 3	4.8	4.839	4.725	4.789	4.139
26	$5b_{15}$	n-Pr	$PhCH_2CH_2$	H	52 ± 3	8.7	4.585	4.565	4.580	4.235
27	$5b_{16}$	n-Bu	$PhCH_2CH_2$	H	59 ± 6	9.8	4.530	4.588	4.547	4.444
28	$5b_{17}$	Ph	$PhCH_2CH_2$	H	Nc	57.0	3.767	3.832	3.779	4.182
29	$5b_{18}$	CH_2Ph	$PhCH_2CH_2$	H	Nc	57.0	3.767	3.755	3.750	3.773
30	$5b_{19}$	Me	p-$MeOPhCH_2CH_2$	H	153 ± 13	25.5	4.116	4.096	4.078	4.189
31	$5b_{20}$	Et	p-$MeOPhCH_2CH_2$	H	89 ± 10	14.8	4.352	4.151	4.163	4.325
32	$5b_{21}$	n-Pr	p-$MeOPhCH_2CH_2$	H	267 ± 18	44.5	3.875	4.075	4.117	4.293
33	$5b_{22}$	n-Bu	p-$MeOPhCH_2CH_2$	H	93 ± 7	15.5	4.333	4.385	4.329	4.321
34	$5b_{23}$	CH_2Ph	p-$MeOPhCH_2CH_2$	H	Nc	73.0	3.660	3.668	3.686	4.029

Table 1. (Contd.)

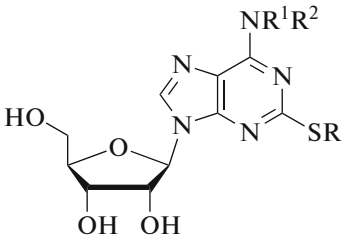

Entry	Compd.	R	R^1	R^2	IC_{50}, μM[a]	PAC (%, 300 μM) [c]	log(PAC)	Predicted log(PAC)		
								CoMFA	CoMSIA	SoMFA2
35*	$5b_{24}$	Me	*m*-$MeOPhCH_2CH_2$	H	Nc	71.0	3.672	4.599	4.532	4.147
36	$5b_{25}$	Et	*m*-$MeOPhCH_2CH_2$	H	38 ± 4	6.3	4.721	4.649	4.643	4.361
37	$5b_{26}$	*n*-Pr	*m*-$MeOPhCH_2CH_2$	H	69 ± 5	11.5	4.462	4.551	4.530	4.353
38	$5b_{27}$	*n*-Bu	*m*-$MeOPhCH_2CH_2$	H	Nc	85.0	3.594	3.551	3.568	3.985
39	$5b_{28}$	Et	$CH(CH_3)Ph$	H	197 ± 12	32.8	4.007	3.999	4.001	3.956
40	$5b_{29}$	*n*-Pr	$CH(CH_3)Ph$	H	Nc	82.0	3.609	3.617	3.622	3.788
41	$5b_{30}$	Me	*p*-$CH_2CH_2C_6H_4F$	H	Nc	57.0	3.767	3.725	3.680	3.964
42	$5b_{31}$	Et	*p*-$CH_2CH_2C_6H_4F$	H	Nc	74.0	3.654	3.755	3.744	3.907
43	$5b_{32}$	*n*-Pr	*p*-$CH_2CH_2C_6H_4F$	H	Nc	52.0	3.807	3.787	3.812	4.114
44	$5b_{33}$	Et	*p*-$CH_2C_6H_4F$	H	Nc	90.0	3.569	3.626	3.563	3.874
45*	$5b_{34}$	*n*-Pr	*p*-$CH_2C_6H_4F$	H	Nc	69.0	3.684	3.401	4.129	3.991

[a] IC_{50} values are expressed as mean ± SEM. ($n = 3$) and calculated when platelet aggregation was below 50% of control (10 μM ADP as agonist). [b] Nc, not calculated, because maximal inhibition of aggregation was lower than 50% at final concentration of 300 μM (10 μM ADP as agonist). [c] PAC, platelet aggregation of control; the inhibition of aggregation at final concentration of 300 μM (10 μM ADP as agonist). * Represent test set compounds, others are training set.

Except for steric (S) and electrostatic (E) fields, there are also three fields—hydrophobic property (H), hydrogen bond donor (D), and hydrogen bond acceptor (A)—used to build models in the CoMSIA method. Adjusting column filtering from 0.5 to 6 kcal/mol would improve efficiency and decrease the noise. And the remaining parameters are the system defaults. According to permutation and combination of five descriptors, 45 generated models were prepared for further 3D-QSAR analysis.

In this study, the partial least square (PLS) method [22] was used to relate the CoMFA and CoMSIA descriptors (as independent variables) to the activity values (log(PAC)) of training set (as dependent variables) so as to build the 3D-QSAR models. To validate the predictive ability of the built model by PLS, the cross-validation analysis was performed using the leave one out (LOO) method. Then the cross-validation correlation coefficient (q^2) indicates predicative power and robustness of built models. Some PLS models with cross-validation analysis were accomplished in different components number to derive the ONC (optimum number of components) with the lowest standard error of estimate (SEE). According to

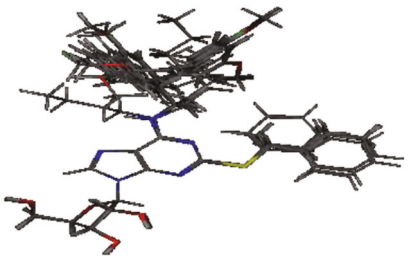

Fig. 2. Superposition of molecules using alignment A. Superposition of all compounds.

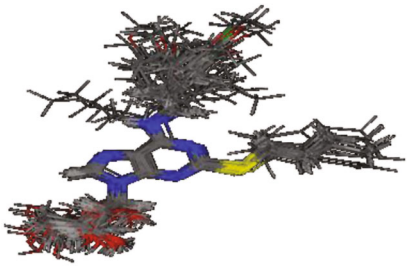

Fig. 3. Superposition of molecules using alignment B. Superposition of all compounds.

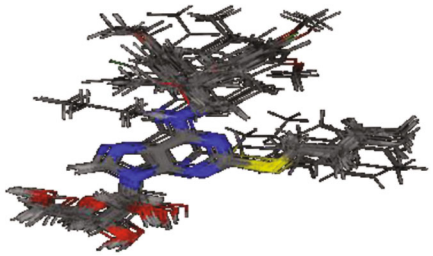

Fig. 4. Superposition of molecules using alignment C. Superposition of all compounds.

the optimum number of components, PLS analysis wa then followed with non-cross-validation as final modelling tool and a series of statistical parameter were obtained, such as the squared correlation coefficient (r^2), standard error of estimate (SEE), and F values. Finally, the predictive abilities of built models were validated using the test set.

The three different alignment CoMFA models were obtained based on training set consisting of 40 compounds to analyze the relationship between chemical structures and antiplatelet aggregation activity; the statistical parameters associated with CoMFA are summarized in Table 2.

The specific parameters of the best CoMFA model (alignment A) are as follows: the cross-validated q^2 of 0.560 with seven components, non-cross-validated r^2 of 0.940, F = 71.850, and SEE of 0.090. The contributions of the steric and electrostatic fields were 59.4 and 40.6%, respectively. The predicted log(PAC) values of best models calculated by CoMFA are listed in Table 1. The correlation between experimental and predicted log(PAC) values by CoMFA model is shown in Fig. 5a. The high F and r^2 with lower SEE value indicates that the model has appropriate reliability and predictive ability.

Compound 25 displayed in Fig. 6 to aid visualization. For the best CoMFA model, the steric and electrostatic contour maps are shown in Figs. 7a, 7b. In Fig. 7a, the green contour parts (80% contributions) indicating the bulky groups would increase the activities and yellow contour parts (20% contributions) showing the bulky groups were unfavorable groups. In Fig. 7b, blue and red contour parts (80% and 20% contributions) represented positively and negatively charged groups that were favorable for activities, respectively.

According to the steric contour maps in Fig. 7a, great green contours appears at the end of region A, which indicates that bulky group in this position would increase activity. For example, incompounds **22** and **14** listed in Table 1 terminal structure of substitute R^1 changes from –H to –OMe; log(PAC) values (4.043 > 3.967) increase with increase in the size of the substitutes (–H < –OMe). At the same time, yellow contours surrounding the middle part of region A indicate that the bulky group in this position would decrease activity, and then bulky group in region A can not be connected to C-6 position of purine ring directly, suggesting connection through gracile link groups. Compound **13** and **39** listed in Table 1 have substitutes

Table 2. Statistical results of CoMFA and CoMSIA models

	COMFA			COMSIA		
	alignment A	alignment B	alignment C	alignment A	alignment B	alignment C
q^{2a}	0.560	0.058	0.048	0.528	0.120	0.157
ONC[b]	7	1	2	4	2	4
r^{2c}	0.940	0.506	0.375	0.943	0.556	0.676
SEE[d]	0.097	0.260	0.293	0.108	0.250	0.216
F[e]	71.850	38.976	11.081	29.290	23.141	18.294
S[f]	59.4	49.3	58.2	6.1	–	15.3
E[f]	40.6	50.7	41.8	16.2	26.7	39.0
H[f]	–	–		39.7	73.3	33.0
D[f]	–	–		38.0	–	10.0
A[f]	–	–		–	–	2.7
r^2_{pred}[g]	0.092 (0.712)	–	–	0.097 (0.766)	–	–

[a]q^2, cross-validated correlation coefficient. [b]ONC, optimum number of components from PLS analysis. [c]r^2, non-cross-validated correlation coefficient. [d]SEE, standard error of estimate. [e]F, the value of F statistic. [f]Field contributions: steric (S), electrostatic (E), hydrophobic (H), hydrogen bond donor (D), and gydrogen bond acceptor (A) fields. [g]Predictive r^2 of all test set compounds (CoMFA: compound **35** classified as outlier; CoMSIA: compound **25** classified as outlier).

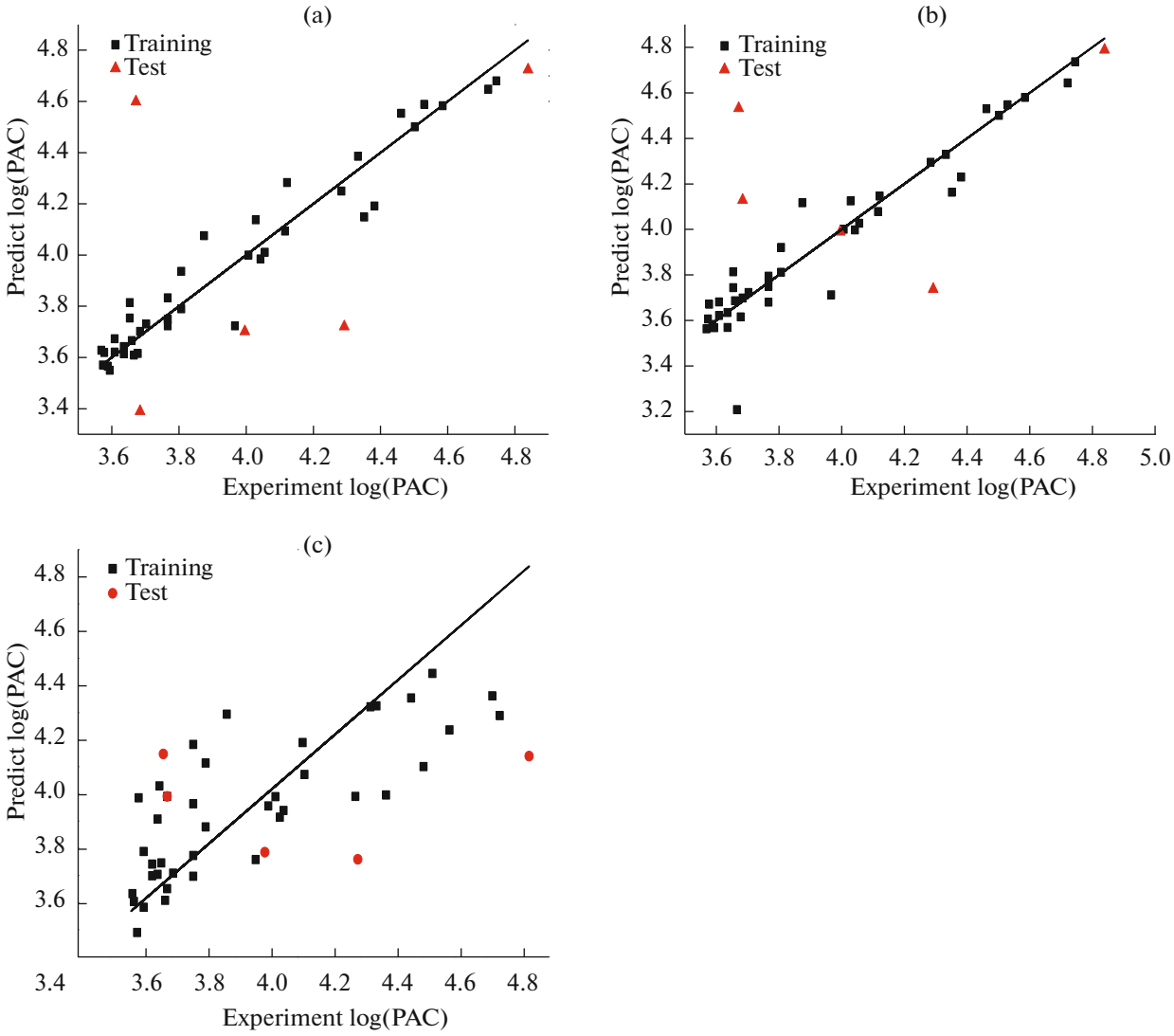

Fig. 5. Correlation between experimental and predicted activities of the best CoMFA and CoMSIA models. (a) CoMFA; (b) CoMSIA; and (c) SOMFA.

varying from $-CH_2Ph$ to $-CH(CH_3)Ph$; the increase of size of substitutes R^1 ($-CH_2Ph < -CH(CH_3)Ph$) however resulted in the decrease of log(PAC) values (4.056 > 4.007). There is a small yellow polyhedron near the ethylthio group in region B, indicating that small groups would increase the activity.

In Fig. 7b, the appearance of the two large blue contours near the region A, one blue contour close to the amino group and the other around the terminal of phenyl rings, indicates that groups with positive charge would increase the activity. For example, structures of substituents in compounds **13** and **2** changed from $-CH_2Ph$ to $-c\text{-}C_6H_{11}$ ($-CH_2Ph < -c\text{-}C_6H_{11}$); the activity increased respectively (4.056 < 4.284), due to the increasing of electron-donating potency in substituent at position 6. It also can be seen from Fig. 7b that there is a red region appearing below the benzene ring. This red contour indicates that the electron-withdrawing group could decrease the activity (log(PAC)). In compounds **24** and **30**, when structures changed from $-H$ to $-OMe$ ($-H < -OMe$, $-OMe$, an electron-donating group), the activity decreased respectively (4.745 > 4.166), due to the decreasing of electron-withdrawing potency in substituent at position 6. In Fig. 7b, there are still some small blue contours near the sugar ring in region C, which indicates that more hydroxyl groups with positive charge would increase the activity.

To constrcut CoMSIA models, there are also three different alignments applied in training set for the combinations of different descriptors. Five CoMSIA descriptors dependency would reduce the model significance and predictive ability [23]. Therefore, all 31 possible combinations of descriptors were calculated

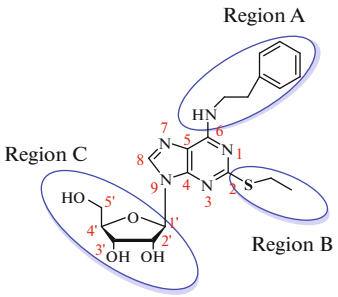

Fig. 6. Structure of template compound (the most active molecule **25**), the three depicted regions A, B, and C, and the number of each substituent position in the purine ring.

with their respective q^2 value and optimum number of components shown in Fig. 8. Electrostatic, steric, hydrogen bond donor, and hydrophobic fields present the highest q^2 value (0.528) and were thus selected to create the final CoMSIA model.

The statistical parameters obtained by the best CoMSIA model for different alignments are listed in Table 2. The model of alignment A provided the high q^2 and r^2 value of 0.528 and 0.943 with optimized components of 14. The derived values for the best model (CoMSIA) are fulfilling the threshold criteria. The contributions of hydrogen bond donor, hydrophobic, steric, and electrostatic fields were 38.0, 39.7, 6.1, and

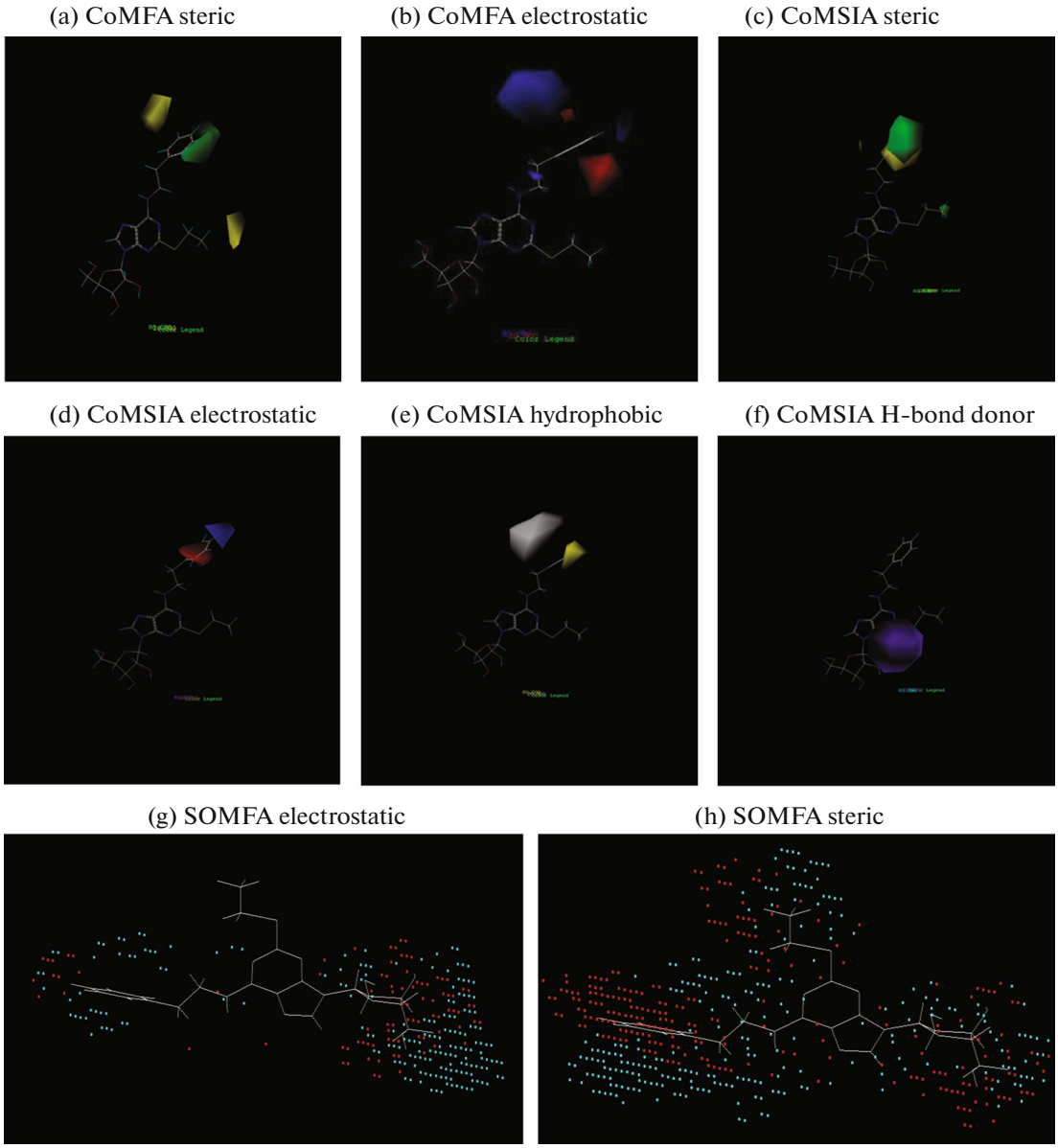

Fig. 7. Contour maps of CoMFA and CoMSIA: (a) CoMFA steric; (b) CoMFA electrostatic; (c) CoMSIA steric; (d) CoMSIA electrostatic; (e) CoMSIA hydrophobic; (f) CoMSIA H-bond donor electrostatic; (g) SOMFA electrostatic; (h) SOMFA steric fields based on compound **25**.

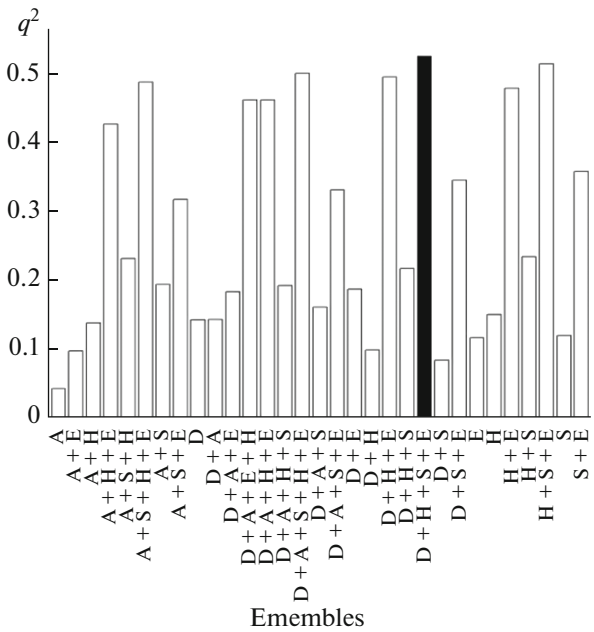

Fig. 8. Graph of the 31 possible CoMSIA descriptors combinations (S = steric, E = electrostatic, H = hydrophobic, D/A = H-bond donor/acceptor) with their respective q^2 values, optimal numbers of components are reported above bars.

16.2%, respectively. In this model, the hydrophobic field was found to have higher contributions to the activity. The predicted log(PAC) values calculated by this CoMSIA model are also given in Table 1. The log(PAC) values of compounds of the test set were also predicted by this model. The correlation plot of predicted and experimental log(PAC) values were shown in Fig. 5b.

The contour maps of CoMSIA fields (steric, electrostatic, hydrophobic, and hydrogen bond donor) with compound **25** are shown in Fig. 7. As shown in Fig. 7d, the contour maps of CoMSIA fields (steric, electrostatic) were basically similar to those of the CoMFA method; for example, small groups with positive charge (such as alkyl amino group) near C-6 position of purine ring and bulky electron withdrawing group (such as phenyl rings with –F, –Cl, –Br, and $-NO_2$) far away from C-6 position of purine ring in region A would increase the activity. Therefore, only contour maps of hydrophobic and hydrogen bond donor fields are discussed in detail.

In hydrophobic field contour maps, yellow and gray contours showed the regions where hydrophobic groups were advantageous and disadvantageous for activity, respectively. As shown in Fig. 7e, the appearance of yellow contours at C-6 position of purine ring in region A indicates that terminal hydrophobic substituent would increase the activity. For example, the inhibitory activity of compound **14** containing *p*-methoxy group was better than that of compounds **22** and **15** not having *p*-methoxy group. This phenomenon agreed with the fact of the CoMFA steric field.

Hydrogen bond donor contour maps of CoMSIA models are shown in Fig. 7f. Cyan and purple contours represent regions where hydrogen bond donor groups would be favorable and unfavorable for activity, respectively. As displayed in Fig. 7f, there is a large cyan contour near the C-2 position of purine ring, suggesting that the hydrogen bond donor substituents in region A would increase the activity. The findings also support our prior research conclusion: the compounds substituted with alkylamino groups possess higher antiplatelet aggregation inhibitory activities than the compounds substituted with alkoxyl groups [24].

For SOMFA models, we added five different charges (DELRE, PULLMAN, GASTEIGER, GAST_HUCK, MMFF94) to three different alignments to establish fifteen models. In SOMFA2 software, we calculated the electrostatic and steric fields of fifteen models with two resolutions of grid (0.5, 1.0 Å) inside a three-dimensional (coordinate origin: –20, –20, –20; volume: 40 × 40 × 40 Å). The nonlinear equation ($\log(PAC) = c_1\log(PAC)_{ESP} + (1 - c_1) \times \log(PAC)_{shap}$) was used to measure the effects of electrostatic and steric fields. The c_1 of all thirty models was calculated. At the same time, we got the corresponding values of SEE, F value, r^2, r^2_{cv}, and r^2_{pred} listed in Table 3.

For Table 3, it is obvious that the twelfth model is the best model with highest r^2_{cv} value of 0.577 which indicates that the model can provide high predictability; and the predicted activities (log(PAC)) are listed in Table 1. An optimal coefficient $c_1 = 0.154$ indicted that the steric contribution has high importance. The liner relation graph of experiment and predict log(PAC) value are shown in Fig. 5c, including the training and test set, with liner correlation coefficient 0.615 and 0.003 (0.781) (predicted r^2 of all test or compound **25** as outliner).

For SOMFA models, the contour maps of electrostatic and steric fields of compound **25** are also shown in Fig. 7. In Fig. 7g, the red grid dots at the C-5' position indicate that a positive charge is favorable in this region and the blue indicates that a negative charge is favorable in this region. In Fig. 7h, the red grid dots at the C-2, C-6, and C-5' positions indicate that steric bulk enhances the activity and the blue ones decrese the activity in these regions.

Based on the above analysis of CoMFA, CoMSIA, and SOMFA method, we found many effects of each group as a substitute in the region A, B, and C. The results show that the inhibitory activities could be enhanced by introduction of medium-sized groups at the C-2 position of the purine ring; long groups with strong electronegativity at the C-6 position of the purine ring and more hydrogen bonding donor groups at the C-5' position of the sugar ring. Taking align-

Table 3. Statistical results of SOMFA models with different alignments, charges, and resolution of grid

Model no.	Alignment	Charge	Resolution of grid, Å	c_1[a]	s[b]	F[c]	r^2[d]	r^2_{cv}[e]	r^2_{pred}[f]
1	A	DELRE	0.5	0.830	0.295	29.252	0.348	0.291	0.056 (0.003)
2	A	DELRE	1.0	1.005	0.284	24.857	0.395	0.343	0.039 (0.000)
3	A	PULLMAN	0.5	0.825	0.296	19.680	0.341	0.275	0.049 (0.034)
4	A	PULLMAN	1.0	0.918	0.289	22.665	0.374	0.308	0.035 (0.033)
5	A	GASTEIGER	0.5	0.707	0.297	19.229	0.336	0.278	0.050 (0.013)
6	A	GASTEIGER	1.0	0.782	0.293	20.906	0.355	0.299	0.041 (0.009)
7	A	GAST_HUCK	0.5	0.681	0.298	18.932	0.333	0.268	0.047 (0.035)
8	A	GAST_HUCK	1.0	0.792	0.295	20.104	0.356	0.283	0.042 (0.027)
9	A	MMFF94	0.5	0.833	0.304	16.792	0.306	0.240	0.096 (0.006)
10	A	MMFF94	1.0	1.173	0.298	19.107	0.335	0.273	0.063 (0.013)
11	B	DELRE	0.5	0.167	0.230	57.534	0.602	0.564	0.001 (0.679)
12	**B**	**DELRE**	**1.0**	**0.154**	**0.226**	**60.797**	**0.615**	**0.577**	**0.003 (0.781)**
13	B	PULLMAN	0.5	0.114	0.234	54.864	0.591	0.551	0.001 (0.658)
14	B	PULLMAN	1.0	0.105	0.229	58.322	0.605	0.566	0.015 (0.773)
15	B	GASTEIGER	0.5	0.110	0.233	55.037	0.592	0.551	0.001 (0.673)
16	B	GASTEIGER	1.0	0.091	0.229	58.192	0.605	0.565	0.004 (0.777)
17	B	GAST_HUCK	0.5	0.027	0.230	53.693	0.586	0.545	0.000 (0.670)
18	B	GAST_HUCK	1.0	0.010	0.231	57.160	0.601	0.561	0.008 (0.782)
19	B	MMFF94	0.5	0.147	0.233	55.424	0.593	0.554	0.000 (0.668)
20	B	MMFF94	1.0	0.143	0.168	59.057	0.608	0.569	0.010 (0.778)
21	C	DELRE	0.5	0.008	0.292	21.234	0.358	0.292	0.002 (0.353)
22	C	DELRE	1.0	0.008	0.294	20.500	0.350	0.283	0.005 (0.321)
23	C	PULLMAN	0.5	0.043	0.294	20.520	0.351	0.284	0.002 (0.353)
24	C	PULLMAN	1.0	0.043	0.294	20.645	0.352	0.285	0.005 (0.321)
25	C	GASTEIGER	0.5	0.008	0.292	21.234	0.358	0.292	0.002 (0.353)
26	C	GASTEIGER	1.0	0.006	0.294	20.531	0.351	0.284	0.005 (0.321)
27	C	GAST_HUCK	0.5	0.008	0.292	21.234	0.358	0.292	0.002 (0.353)
28	C	GAST_HUCK	1.0	–0.140	0.294	20.520	0.351	0.284	0.004 (0.315)
29	C	MMFF94	0.5	0.246	0.291	21.882	0.365	0.301	0.015 (0.453)
30	C	MMFF94	1.0	0.202	0.293	20.898	0.355	0.289	0.012 (0.421)

[a]Mixing coefficient of the SOMFA model. [b]Standard error of the estimate. [c]F-test value. [d]Non-cross-validated correlation coefficient. [e]Cross-validated correlation coefficient. [f]Predictive r^2 of all test set compounds (compound **25** classified as outlier).

ments into account, we found that the alignment had a profound influence on the result. The model which was built by alignment A showed the highest values of r^2 and q^2 because it reflected the fact that purine ring was the true basic backbone of adenosine derivatives.

The most potent compound **25** was regarded as the reference molecule, and the new compounds could be designed by replacing favorable groups at each position of compound **25**. These findings can be applied to design new adenosine derivatives with bulky group at position 6 in region A with higher electron withdrawing ability, such as F, Cl, Br, and $-NO_2$, and the stronger hydrogen bond donor groups at position C-5', such as $-COOH$, $-CH_2OH$, etc.

ACKNOWLEDGMENTS

The authors gratefully acknowledge professor Lei Ming. We also thank the Chemical Grid Project at Beijing University of Chemical Technology (BUCT) for providing a part of the computational resources. By analyzing the corresponding contour maps detailly, new adenosine derivatives with potential efficacy were designed for synthesis in the future.

FUNDING

This work was supported by the National Natural Science Foundation of China (no. 21272022).

COMPLIANCE WITH ETHICAL STANDARDS

The work has no studies involving humans or animals as subjects of the study.

Conflict of Interests

Authors declare they have no conflicts of interest.

REFERENCES

1. Flügel, K.A., *Fortschr. Med.*, 1980, vol. 98, pp. 773–778.
2. Wood, D.A., *Lancet*, 2001, vol. 357, pp. 995–1001.
3. Gould, W.R. and Leadley, R.J., *Curr. Pharm. Design*, 2003, vol. 9, pp. 2337–2347.
4. Lip, G.Y., Felmeden, D.C., and Dwivedi, G., *Cochrane Db. Syst. Rev.*, 2011, vol. 8, CD003186.
5. Springthorpe, B., Bailey, A., Barton, P., Birkinshaw, T.N., Bonnert, R.V., Brown, R.C., Chapman, D., Dixon, J., Guile, S.D., Humphries, R.G., Hunt, S.F., Ince, F., Ingall, A.H., Kirk, I.P., Leeson, P.D., Leff, P., Lewis, R.J., Martin, B.P., McGinnity, D.F., Mortimore, M.P., Paine, S.W., Pairaudeau, G., Patel, A., Rigby, A.J., Riley, R.J., Teobald, B.J., Tomlinson, W., Webborn, P.J., and Willis, P.A., *Bioorg. Med. Chem. Lett.*, 2007, vol. 17, pp. 6013–6018.
6. Fosburgh, D., *Mayo Clin. Proc.*, 2006, vol. 81, pp. 989–989.
7. Savi, P. and Herbert, J.M., *Haematologica*, 2000, vol. 85, pp. 73–77.
8. Husted, S. and van Giezen, J.J., *Cardiovasc. Ther.*, 2009, vol. 27, pp. 259–274.
9. Ingall, A.H., Dixon, J., Bailey, A., Coombs, M.E., Cox, D., McInally, J.I., Hunt, S.F., Kindon, N.D., Teobald, B.J., Willis, P.A., Humphries, R.G., Leff, P., Clegg, J.A., Smith, J.A., and Tomlinson, W., *J. Med. Chem.*, 1999, vol. 42, pp. 213–220.
10. Ferreiro, J.L., Ueno, M., and Angiolillo, D.J., *Expert Rev. Cardiovasc. Ther.*, 2009, vol. 7, pp. 1195–1201.
11. Langlois, M., Brémont, B., Rousselle, D., and Gaudy, F. *Eur. J. Pharmacol.: Mol. Pharmacol.*, 1993, vol. 244, pp. 77–87.
12. Jiang, H.L., Chen, K.X., Wang, H.W., Tian, Y., Chen, J.Z., and Ji, R.Y., *Acta Pharmacol. Sin.*, 1994, vol. 15, pp. 481–487.
13. Sperandio, G.M., Sant'Anna, C.M., Barreiro, E., *J. Bioorgan. Med. Chem.*, 2004, vol. 12, pp. 3159–3166.
14. Caballero, J., *J. Mol. Graph. Model.*, 2010, vol. 29, pp. 363–371.
15. Zhang, J., Wang, X.J., Dong, Z.K., Wang, S.Q., Xu, W.R., Fu, J.W., Cheng, X.C., and Wang, R.L., *Lett. Drug Des. Discov.*, 2016, vol. 13, pp. 376–386.
16. Cramer, R.D., Patterson, D.E., and Bunce, J.D., *J. Am. Chem. Soc.*, 1988, vol. 110, pp. 5959–5967.
17. Klebe, G., Abraham, U., and Mietzner, T., *J. Med. Chem.*, 1994, vol. 37, pp. 4130–4146.
18. Li, Z., Zhou, M., Wu, F., Li, R., and Ding, Z., *Eur. J. Med. Chem.*, 2011, vol. 46, pp. 58–64.
19. Liu, G., Xu, J., Chen, N., Zhang, S., Ding, Z., and Du, H., *Eur. J. Med. Chem.*, 2012, vol. 53, pp. 114–123.
20. Zhao, L.J., Zhang, L.R., and Lei, M., *Sci. China Chem.*, 2013, vol. 56, pp. 1550–1563.
21. Gasteiger, J. and Marsili, M., *Tetrahedron*, 1980, vol. 36, pp. 3219–3228.
22. Wold, S., Ruhe, A., Wold, H., and Dunn III, W.J., *Siam J. Sci. Stat. Comput.*, 1984, vol. 5, pp. 735–743.
23. Bringmann, G. and Rummey, C., *J. Chem. Inf. Comput. Sci.*, 2003, vol. 43, pp. 304–316.
24. Du, H.G., Yu, M.W., Deng, C.E., Lu, C.H., and Li, S.L., *J. Heterocycl. Chem.*, 2016, vol. 54, pp. 436–449.